# Ultrafast Roaming Mechanisms in Ethanol Probed by Intense Extreme Ultraviolet Free-electron Laser Radiation: Electron Transfer Versus Proton Transfer

Enliang Wang [*,†,‡] Nora G Kling,[¶] Aaron C LaForge,[¶] Razib Obaid,[¶] Shashank Pathak [†] Surjendu Bhattacharyya [†] Severin Meister,[§] Florian Trost,[§] Hannes Lindenblatt,[§] Patrizia Schoch,[§] Matthias Kübel,[‖,⊥] Thomas Pfeifer,[§] Artem Rudenko,[†] Sergio Díaz-Tendero [#,@,△] Fernando Martín [#,@,∇] Robert Moshammer,[§] Daniel Rolles [†] and Nora Berrah [*,¶]

†*J. R. Macdonald Laboratory, Department of Physics, Kansas State University, Manhattan, KS, USA*

‡*Hefei National Research Center for Physical Sciences at the Microscale and Department of Modern Physics, University of Science and Technology of China, Hefei 230026, China*

¶*Physics Department, University of Connecticut, Storrs, CT, USA*

§*Max Planck Institut für Kernphysik, Saupfercheckweg 1, 69117 Heidelberg, Germany*

‖*Institute of Optics and Quantum Electronics, Friedrich Schiller University Jena, D-07743 Jena, Germany*

⊥*Helmholtz Institute Jena, Fröbelstieg 3, 07743 Jena, Germany*

#*Departamento de Química, Módulo 13, Universidad Autónoma de Madrid, 28049 Madrid, Spain*

@*Condensed Matter Physics Center (IFIMAC), Universidad Autónoma de Madrid, 28049 Madrid, Spain*

△*Institute for Advanced Research in Chemical Sciences (IAdChem), Universidad Autónoma de Madrid, 28049 Madrid, Spain*

∇*Instituto Madrileño de Estudios Avanzados en Nanociencia (IMDEA-Nano), Campus de Cantoblanco, 28049 Madrid, Spain*

E-mail: enliang@phys.ksu.edu,elwang@ustc.edu.cn; nora.berrah@uconn.edu

**Abstract**

Ultrafast $H_2^+$ and $H_3^+$ formation from ethanol is studied using pump-probe spectroscopy with an extreme ultraviolet (XUV) free-electron laser. The first pulse creates a dication, triggering $H_2$ roaming that leads to $H_2^+$ and $H_3^+$ formation, which is disruptively probed by a second pulse. At photon energies of 28 and 32 eV, the ratio of $H_2^+$ to $H_3^+$ increases with time delay, while it is flat at a photon energy of 70 eV. The delay-dependent effect is ascribed to a competition between electron and proton transfer. High-level quantum chemistry calculations show a flat potential energy surface for $H_2$ formation, indicating that the intermediate state may have a long lifetime. The *ab initio* molecular dynamics simulation confirms that, in addition to the direct emission, a small portion of $H_2$ undergoes a roaming mechanism that leads to two competing pathways: electron transfer from $H_2$ to $C_2H_4O^{2+}$ and proton transfer from $C_2H_4O^{2+}$ to $H_2$.

# TOC Graphic

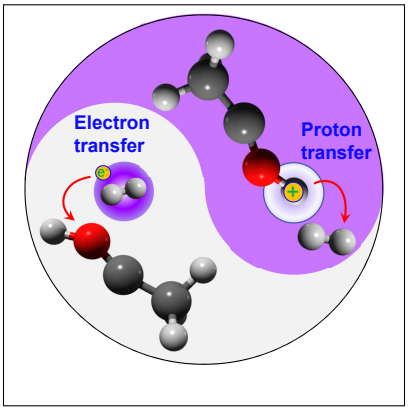


# Keywords

Proton transfer, Electron transfer, FEL, Coulomb Explosion, Roaming, Disruptive probing, Coincidence ion momentum imaging

Charge transfer, charge migration, and charge separation between the atomic centers of a molecule are crucial steps in chemical bond formation and dissociation, and also play an important role in internal conversion.[1–7] When triggered by photoabsorption or particle impact, the change in the molecular electronic structure induces nuclear motion, which can result in substantial changes in molecular geometry,[8] e.g. isomerization[9–13] and dissociation.[14] Additionally, the ultrafast charge/hole transfer has an important impact on radiation damage in biological systems, e.g. the DNA mutations induced by proton transfer (PT).[15] To trace the spatial localization of charge at a given time, it is important to create a localized charge at a specific position within a molecule. Due to their element specificity, x-rays can be used to create such a localized hole.[2,4] Therefore, recently developed free-electron-laser (FEL) pump-probe techniques[1–3] have opened up promising ways to trace the charge-transfer processes in space and time with atomic resolution.

A specific topic of interest for recent pump-probe studies with both FELs and table-top optical lasers is roaming-mediated PT[16–19] and the "inverse" harpoon mechanism, which is electron transfer (ET) from the neutral moiety to the dicationic cofragment.[20] During roaming, the molecule dissociates with the fragments transiently moving in each other's proximity, albeit at larger internuclear distances, in contrast to directly following the path predicted by conventional transition-state theory.[21,22] Specifically, roaming chemistry has been observed in neutral hydrogen and hydrogen molecule elimination.[16–19,21,22] For example, roaming-mediated PT was observed in several alcohol dications created by a strong pump pulse and probed by a weak pulse.[16] At the end of the roaming process in the dication, the charges of the system are separated by so called PT-mediated charge transfer,[23] which plays an important role e.g., in biochemistry[24] and astrochemistry.[25–27] In a recent study, Gope et al.[20] indicated that the charges in a dication can also separate by ET. Theoretical calculations show that the timescale of PT is typically on the order of tens of femtoseconds, similar to some electronic decay channels. For example, the simulation by Marsalek et al. showed that in water, the delocalized hole localizes within approximately 30 fs, and PT to

a neighboring water molecule proceeds almost immediately.[28]

If two ultrafast decay mechanisms with comparable timescales occur in the same system, there will be a competition between the two channels.[10,29] Recently, it was found by Richter et al.[30] that PT can close the intermolecular Coulombic decay (ICD)[31] channel in photon-induced inner-valence ionization of water clusters, which shows strong competition between PT and electronic decay. The hypothesis about competition between ET and PT in methanol was mentioned in a study on $H_3^+$ production and Coulomb explosion of methanol by Livshits et al.[18] and Luzon et al.[32] Recently, direct evidence for an ultrafast competition between ET and PT was observed by Gope et al.[20] in the dissociative ionization of methanol.

In this work, we present a combined experimental and theoretical study of the competition between ultrafast ET and PT in the dissociative ionization of ethanol using pump-probe spectroscopy with an XUV FEL. The experiment was performed for three different photon energies, 28, 32, and 70 eV, in order to gain a better understanding of the dynamics. As illustrated in Fig. 1 (a), the ethanol dication is created by the pump pulse, and neutral $H_2$ is formed by an ultrafast isomerization process.[33]

Due to the induced-dipole interaction between the charged and neutral moieties, $H_2$ is weakly bonded to $C_2H_4O^{2+}$ and undergoes a long-range, prolonged roaming. The second FEL pulse acts as a disruptive probe that can interrupt the roaming process before the subsequent PT or ET occurs. In other words, if the probe pulse arrives early enough, it "disrupts" (i.e. dissociates or ionizes) the dicationic $(H_2–C_2H_4O)^{2+}$ precursor, leading to a depletion of the $H_2^+$ and $H_3^+$ channels. For longer time delays, the probe pulse is less likely to disrupt the roaming, thus, the yield of both $H_2^+$ and $H_3^+$ increases until reaching saturation. $H_3^+$ formation occurs when $H_2$ abstracts one proton from either the methyl or the hydroxyl site, while $H_2^+$ is formed via ET from $H_2$ to the dication. Since the formation can occur with slightly different time scales, the ratio of $H_2^+$ to $H_3^+$ will vary, depending on when the roaming process is disrupted.

Here, we use ion momentum imaging to identify those $H_2^+$ and $H_3^+$ ions that are produced

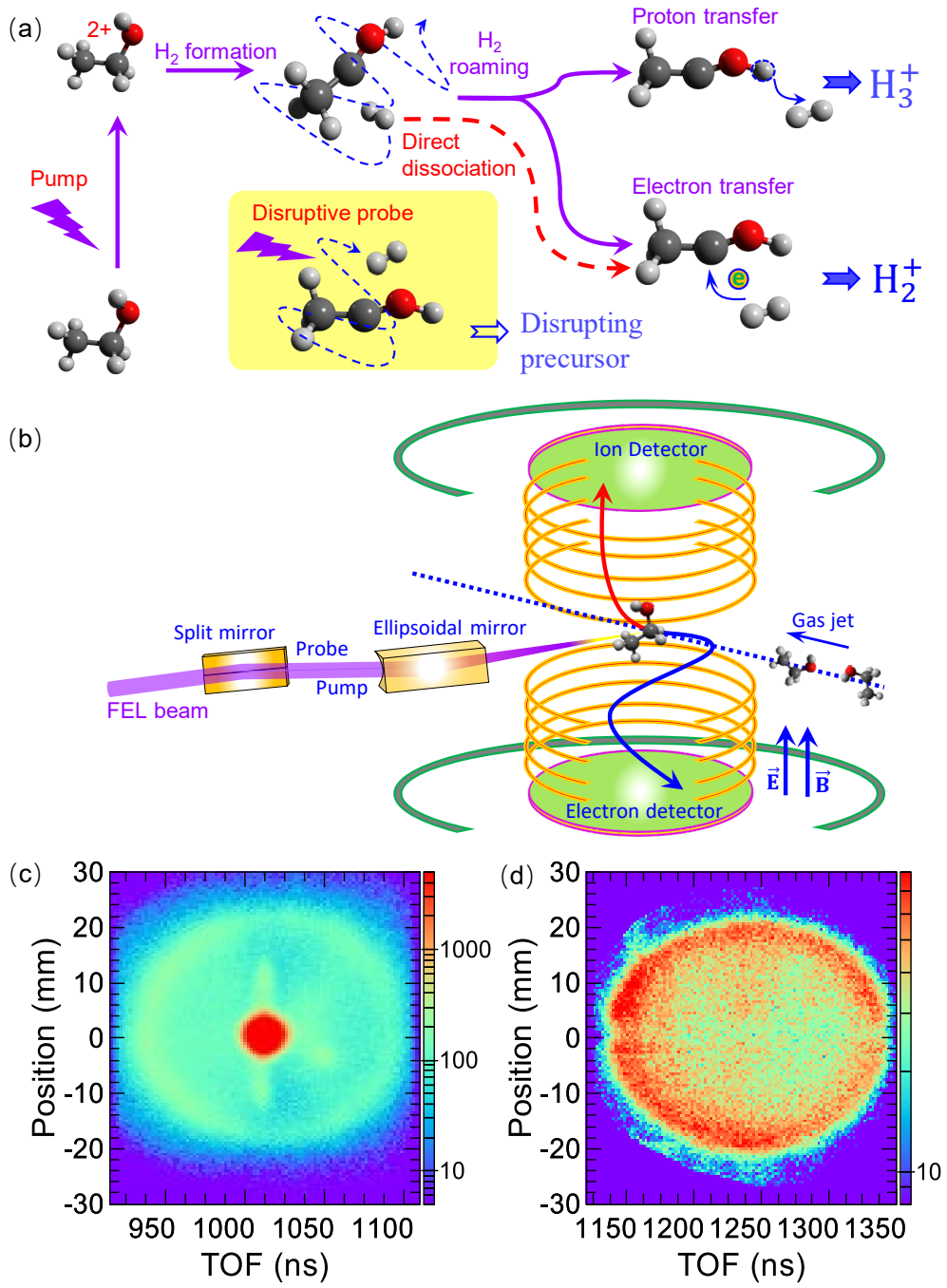


Figure 1: (a) Illustration of the competition between proton and electron transfer in $H_2$ roaming in an ethanol dication. (b) Sketch of the experimental setup. (c) and (d) Position versus time-of-flight image of the $H_2^+$ and $H_3^+$ ions, respectively, produced by photoionization at 28 eV photon energy.

via roaming, by investigating the yields and yield ratios as a function of pump-probe delay. The raw momentum images (displayed as position versus time-of-flight plots) of $H_2^+$ and $H_3^+$

ions produced after ionization at a photon energy of 28 eV are shown in Fig. 1 (c) and (d), respectively. Two structures are observed for $H_2^+$: a nearly isotropic ring, and an intense localized maximum at the center of the distribution. The ring structure corresponds to $H_2^+$ ions with high kinetic energy that originate from the Coulomb explosion of the ethanol dication, while the signal at the center corresponds to low-energy ions that originate from the dissociative single-ionization of ethanol which is not of further interest for the current discussion. For $H_3^+$, we only observe the ring structure which comes from the Coulomb explosion of the ethanol dication. The (central) photon energy of 28 eV is just below the double ionization threshold of 28.2 eV.[34] Hence, the single-photon double-ionization cross-section is very small (it is not zero since the FEL pulses have a combined bandwidth and photon energy jitter of approximately 1%, which just reaches beyond the double ionization threshold). Therefore, at 28 eV, the ethanol dication is predominantly created by a two-photon double-ionization mechanism. The photon energies of 32 and 70 eV are high enough to initiate single-photon double-ionization of ethanol. At 70 eV, the photon energy is high enough to remove an electron from the oxygen 2s orbital, whose ionization potential (approximately 33.5 eV[35]) is higher than the double ionization threshold of ethanol. Hence, at 70 eV, the dication can be created by single-photon inner-valence ionization followed by Auger-Meitner decay. For reference, the O 2s inner valence ionization and double ionization of ethanol and other similar alcohol molecules have been studied by Linusson et al.,[34] Barillot et al.,[36] and Lavín et al.[37]

In order to discuss the energetics of $H_2^+$ and $H_3^+$ formation, Fig. 2 shows the relative energy of several relevant points in the potential energy surface (PES) of doubly charged ethanol. For simplicity, we do not include the complete path to the transition states, only the relevant intermediate structures along with the entrance and exit channels. When ethanol is doubly ionized, a minimum is found in the PES at 26.45 eV as shown by path (1) in Fig. 2. It is formed by an $H_2$ molecule weakly bound to $C_2H_4O^{2+}$. Due to the induced-dipole attraction between the neutral $H_2$ and the doubly charged ion, the molecule cannot dissociate

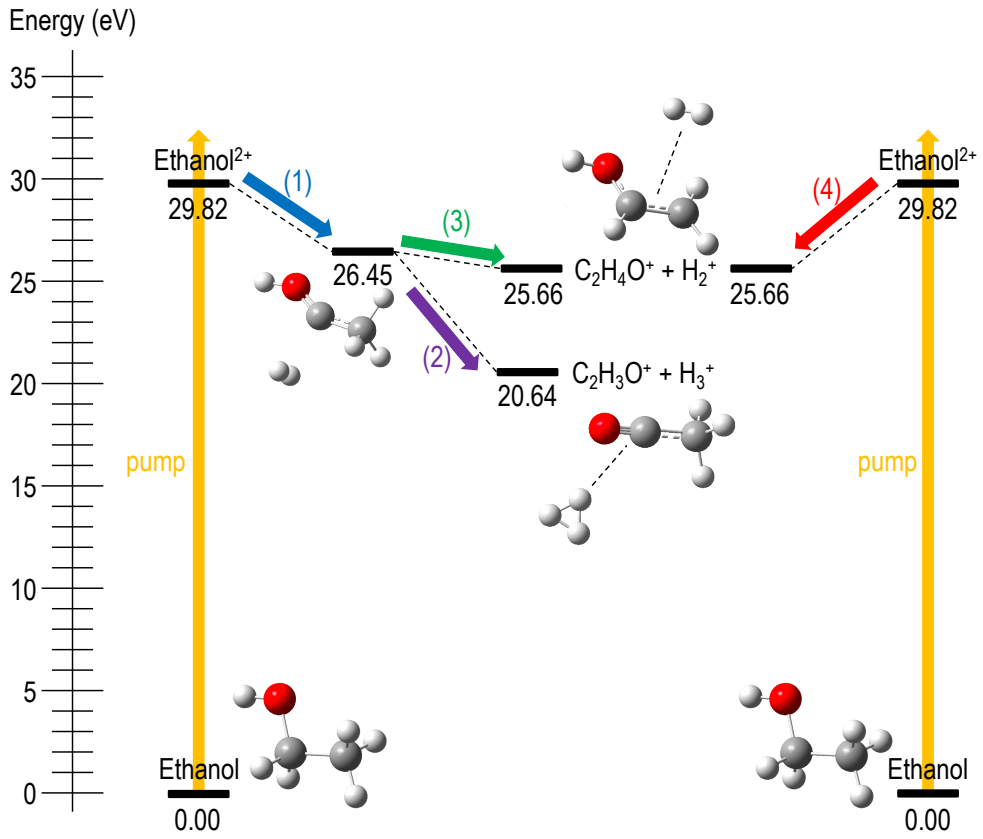


Figure 2: Relevant points in the potential energy surface of the ethanol dication. The potential energy was determined by CCSD(T)/aug-cc-pVTZ theory for the geometries optimized at the B3LYP/6-31++G(d,p) level. Zero-point-energy (ZPE) corrections were made only for the exit channels. The magnitude of the ZPE corrections is approximately 0.2 eV.

directly if the kinetic energy of $H_2$ is not enough to overcome the potential energy barrier. Most likely, roaming occurs in this pathway. After roaming, ET or PT can take place from this intermediate state leading to $H_2^+$ and $H_3^+$ formation as shown by paths (3) and (2) in Fig. 2, respectively. Direct $H_2^+$ formation is also possible if the kinetic energy of the neutral $H_2$ is high enough to quench roaming or if there is no potential energy barrier as shown by channel (4) in Fig. 2 and by the dashed-red curve in Fig. 1 (a). Note that Fig. 2 only includes channels with the most stable structure of $C_2H_4O^+$. The channel $C_2H_3O^+ + H_3^+$ appears at an energy approximately 5 eV lower than $C_2H_4O_2^+ + H_2^+$, thus a higher kinetic energy release (KER) is expected for the $H_3^+$ formation channel.

The experimentally determined KER distributions of the $C_2H_4O^+ + H_2^+$, and $C_2H_3O^+$

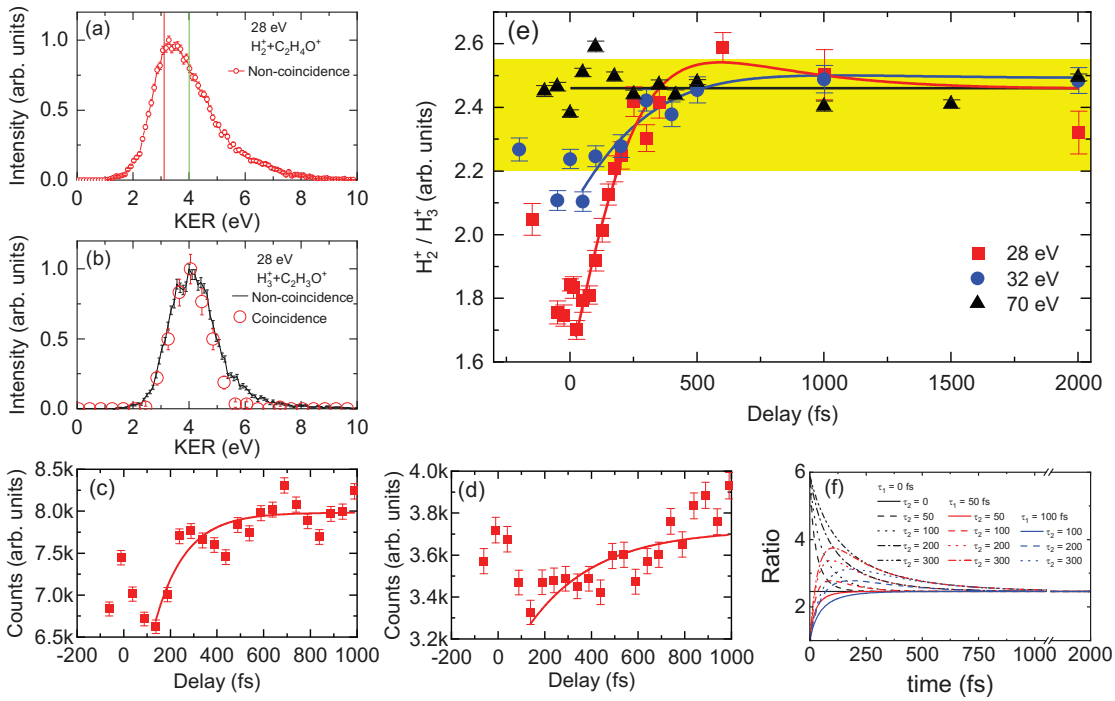


Figure 3: (a) Experimental kinetic energy release of the $C_2H_4O^+ + H_2^+$ channel at 28 eV photon energy. The vertical lines indicate the predictions from the *ab initio* calculation (red) and classical over-the-barrier model (green) for this channel. (b) Experimental kinetic energy releases of the $C_2H_3O^+ + H_3^+$ channel at 28 eV photon energy. The black curves and red circles are the non-coincidence and coincidence data, respectively, as explained in the text. The data are normalized at the maxima. The yields of $H_2^+$ and $H_3^+$ from the dication as a function of delay are shown in (c) and (d), respectively. In this plot, the FEL photon energy is 28 eV. The solid-red curves are exponential fits. (e) Ratio of $H_2^+$ to $H_3^+$ at FEL photon energies of 28, 32, and 70 eV. The red and blue solid lines are fits assuming an exponential increase of the yields. The black line is the average value of the black solid triangles. The yellow band shows the averaged ratio ($2.37 \pm 0.18$) with a 1-$\sigma$ confidence interval of the "probe-pulse-only" results at 28, 32, and 70 eV. (f) Calculated ratio of $H_2^+$ and $H_3^+$ as a function of the time constants.

+ $H_3^+$ channels are shown in Fig. 3 (a) and (b), respectively. Since the kinetic energy distributions of $H_2^+$, and $H_3^+$ are delay-independent (see Supporting Information section I for details), we only show the KERs at 0 fs delay, where data were recorded for the longest time and the statistics are best. For simplicity, we only show the results for an FEL photon energy of 28 eV. The results for 32 eV and 70 eV are shown in section II of the Supporting Information. Due to having poor statistics for the $C_2H_4O^+ + H_2^+$ channel, we have extracted the KER from the high-energy $H_2^+$ signal, i.e., the ring structure in Fig. 1 (c), with the energy of the $C_2H_4O^+$ ion being reconstructed via momentum conservation. Although we do not observe a clear signature of the $C_2H_4O^+ + H_2^+$ coincidence channel in our data due to the strong background from the singly ionized target, it is known from a previous study that this channel does indeed exist.[33] In the case of the $C_2H_3O^+ + H_3^+$ channel, the derivation of the KER from the non-coincident data is cross-checked with the coincident data. This is shown in Fig. 3 (b), where the black curves and the red circles correspond to the results of the reconstruction and coincident measurement, respectively. By normalizing the two results at the maximum, almost identical distributions are observed. From 28 to 70 eV, the KER peaks of $C_2H_4O^+ + H_2^+$ slightly shift at higher energies, i.e. 3.3, 3.4, and 3.6 eV for photon energies of 28, 32, and 70 eV, respectively (see Supporting Information section II for details). For the $C_2H_3O^+ + H_3^+$ channel, almost identical KER peaks at about 4.0 eV are observed, which is higher than the KER of the $C_2H_4O^+ + H_2^+$ channel as mentioned earlier. Interestingly, the experimental KER difference between the PT and ET channels is less than 1 eV, which is much smaller than the predictions from the potential energy surfaces, where the KER of the PT channel is 5 eV higher than the KER of the ET channel, as shown in Fig. 2. This suggests that a large part of the released potential energy is distributed into internal energy degrees of freedom in the PT channel.

To avoid complications that might arise from different detection efficiencies, we use the non-coincident data for both $H_2^+$ and $H_3^+$ Coulomb explosion channels when comparing the yields and the ratio of $H_2^+$ to $H_3^+$ as a function of delay. One further advantage of using

the non-coincident (high-energy) $H_2^+$ and $H_3^+$ ions for this analysis is that, in addition to the two-body Coulomb explosion channel, any multi-body fragmentation channels[38] are also included. The latter channels may result in broader kinetic energy distributions, as shown by the difference between the black line and the red circles in Fig. 3 (b), because more internal energies are involved in these channels. To avoid confusion and denote that only high-energy ions are selected, the experimental non-coincident data of $H_2^+$ and $H_3^+$ are still labeled as $C_2H_4O^+ + H_2^+$ and $C_2H_3O^+ + H_3^+$ channels, respectively.

The delay-dependent ion yields of $H_2^+$ and $H_3^+$ from the dication of ethanol are shown in the Fig. 3 (c) and (d), respectively. The peaks at 0 fs are due to the temporal overlap of the two FEL pulses which enhances multiphoton absorption processes. Similar to the results of Ekanayake et al.,[16] the yields increase exponentially as a function of time. The solid red curves show least-square fits to the exponential function, $y=y_0+A(1-\exp(-t/\tau))$ where $y_0$, A, and $\tau$ are the offset, amplitude, and the time constant, respectively. To avoid the influence of the pump-probe pulses overlap, we fit the data from the first minimum point on the right of the peak centered at time zero. The time constants of $H_2^+$ and $H_3^+$ formation are 132 $\pm$ 43 and 296 $\pm$ 87 fs, respectively. The determined time constants of $H_3^+$ formation channel is in agreement with the results of Ekanayake et al., who reported 235 $\pm$ 10 fs.[16]

As sketched in Fig. 1 (a) and 2, both $H_2^+$ and $H_3^+$ originate from an intermediate neutral $H_2$. The correlation between ET and PT is reflected in the ratio of $H_2^+$ to $H_3^+$, which is shown in Fig. 3 (e). The ratio of $H_2^+$ to $H_3^+$ at the FEL photon energies of 28 and 32 eV increases exponentially with delay, which is evidence of a competition between PT and ET at these photon energies. It is noted that the contrast at 28 eV is higher than at 32 eV. At 70 eV, no time-dependent effect is observed. At 2 ps, the ratios are approximately the same value of 2.5 $\pm$ 0.07, and this asymptotic value is close to the averaged ratio (2.46 $\pm$ 0.02) at 70 eV. We speculate the reason for the constant ratio at 70 eV is related to the Auger-Meitner decay which may create a high degree of internal energy in the molecule due to the ultrafast decay from the excited cationic state to the ground dicationic state. With

increasing internal energy, the lifetime of the metastable $(H_2 - C_2H_4O)^{2+}$ state decreases, thereby preventing the long-time roaming of $H_2$. As a result, the yields of $H_2^+$ and $H_3^+$ at 70 eV already saturate at small time delay, which produces a constant ratio as a function of delay. On the other hand, if there is no Auger decay, the high lying states created by a 70 eV photon are more likely to dissociate the C-O bond rather than to produce the $H_2$ moiety, as shown by Luzon et al.[32] However, further investigation of the C-O bond cleavage is beyond the scope of the present work. The ratios of the single-pulse data ("probe only") are 2.24 ± 0.23, 2.41 ± 0.29, and 2.5 ± 0.23 for 28, 32, and 70 eV, respectively, and their average is shown as a yellow band in Fig. 3(e).

In Fig. 3 (e), the solid-red and solid-blue curves are the fits using the ratios of the exponential functions of $H_2^+$ to $H_3^+$ for 28 and 32 eV, respectively. Overall, there is good agreement between the results and the fit function. In Fig. 3 (f), we plot the simulated ratio as a function of the time constants for $H_2^+$ and $H_3^+$. In this plot, the ratio is calculated using the exponential functions, $y=y_0+A(1-\exp(-t/\tau))$, while keeping the offsets, $y_0$, and amplitudes, A, of both $H_2^+$ and $H_3^+$ as constants, which are obtained by matching the asymptotic to the experimental value. As shown in Fig. 3 (f), at a fixed time constant of $H_2^+$ ($\tau_1$), an increasing time constant of $H_3^+$ ($\tau_2$) delays the time to reach the asymptotic value. In the extreme case of $H_2^+$ and $H_3^+$ being created instantaneously ($\tau_1 = \tau_2 = 0$), the ratio is delay-independent, as shown by the solid black curve in Fig. 3 (f).

To further interpret the correlation between $H_2^+$ and $H_3^+$, we performed potential energy surface calculations and *ab initio* molecular dynamics (AIMD, see Methods for details) simulation for the $H_2$ roaming. We additionally performed model calculations using the classical over-the-barrier (OTB) model[1,2] to determine the average internuclear distance at which ET takes place.

In Fig. 4, we show the results of the molecular dynamics calculations for the formation dynamics of neutral $H_2$, which is the precursor of $H_2^+$ and $H_3^+$. The center-of-mass (COM) distances between $H_2$ and $C_2H_4O^{2+}$ as a function of time are given in Fig. 4 (a)-(c), which

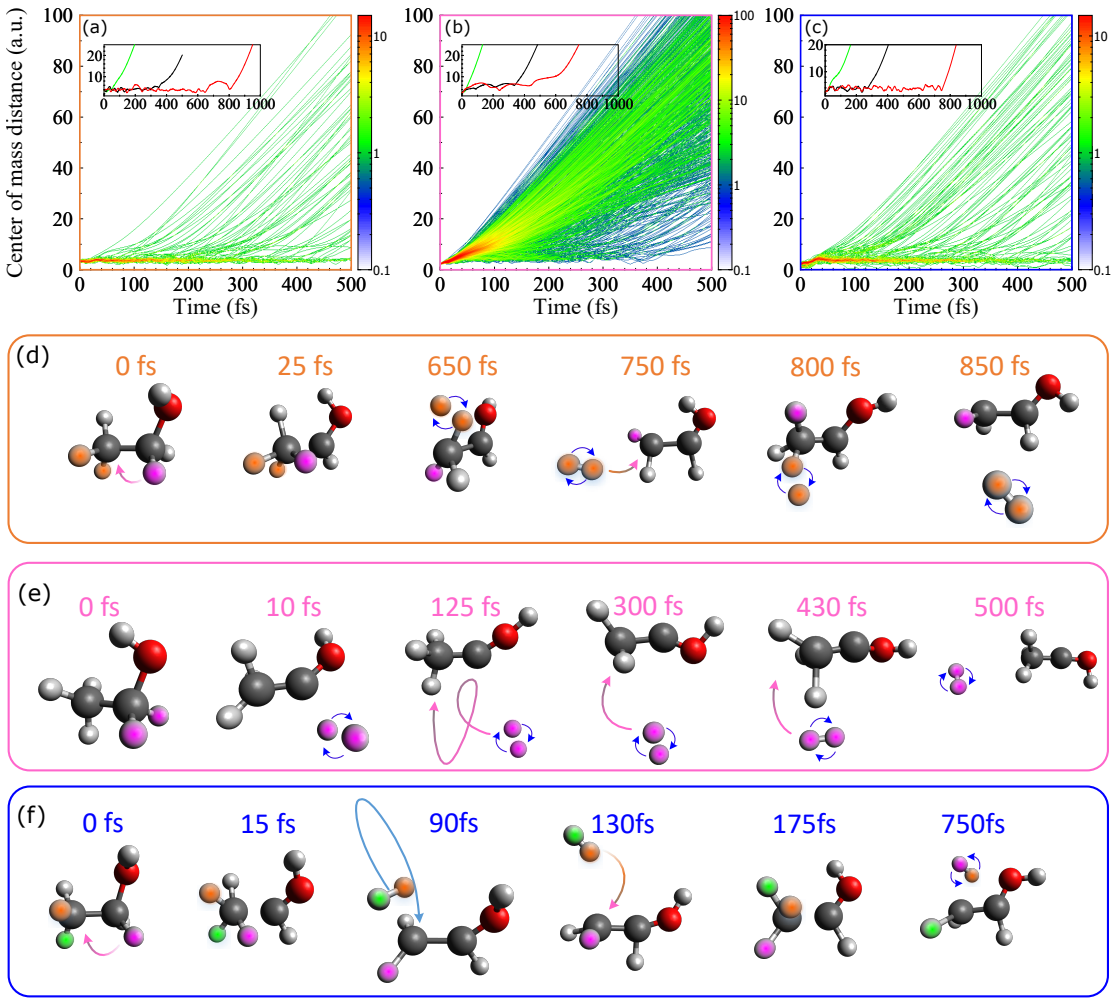


Figure 4: *Ab initio* molecular dynamic simulation of $H_2$ formation. The center-of-mass distance between $H_2$ and $C_2H_4O^{2+}$ for 1226 trajectories as a function of time are shown for $H_2$ originating from the (a) terminal carbon, (b) middle carbon, and (c) for each of the carbons contributing one hydrogen. The green, black, and red curves in the insets show the trajectories with short, middle, and long lifetime, respectively. (d)-(f) Molecular geometries during the trajectories shown in red in the inset of (a)-(c), respectively.

show the cases of $H_2$ originating from the terminal carbon, middle carbon, and when both carbons contribute one hydrogen each, respectively. The insets of Fig. 4 (a)-(c) present three trajectories of direct dissociation, short- and long-time roamings, respectively. Snapshots of the molecular geometries for the red curves in the insets of Fig. 4 (a)-(c) are shown in Fig. 4 (d)-(f), respectively. Due to the complexity of the potential energy surface, there are multiple local energy minima.[33] The direct formation of $H_2$ from the middle carbon creates a potential energy well that is almost barrier-less for dissociation into $H_2$ + $C_2H_4O^{2+}$. PT from the middle to the terminal carbon creates another potential energy well with a barrier of about 2 eV to form a neutral $H_2$ from the transient $CH_4$ group.[33]

In the trajectories shown in Fig. 4 (a)-(c), dissociation of the dication into the $C_2H_4O^{2+}$ + $H_2$ channel begins once the trajectories show a linear increase of the COM distance as a function of time, while the oscillations seen at small COM distances and occuring for an extended time are direct evidence of the roaming mechanism. We can see from Fig. 4 (b) that most of the trajectories dissociate directly and only a small portion undergo roaming. For $H_2$ emission from the terminal carbon, most of the trajectories show long lifetimes, as shown in Fig. 4 (a) and (c). By assigning trajectories where the COM distance remains within 10 a.u. within the first 150 fs to be due to $H_2$ roaming and the rest to direct $H_2$ emission, we can derive a probability of direct and roaming mechanisms of (14%, 86%), (84%, 16%), and (35%, 65%) for Fig. (a), (b) and (c), respectively. It has been shown in previous works[16,33] that $H_3^+$ can only be produced via the $H_2$ roaming mechanism. Thereby, the competition exists on the roaming path: on the one hand, once the neutral $H_2$ comes close enough ($\sim$ 7 a.u.) to the hydroxyl or the methyl group, there could be PT to form $H_3^+$.[33] On the other hand, once the internuclear distance between $C_2H_4O^{2+}$ and $H_2$ approaches the critical distance for ET, there could be ET from $H_2$ to $C_2H_4O^{2+}$, which is in competition with $H_3^+$ formation.

We next turn to the discussion of the ET mechanism. The PES as a function of the COM distance between $H_2$ and $C_2H_4O$ was calculated by means of the extended multistate

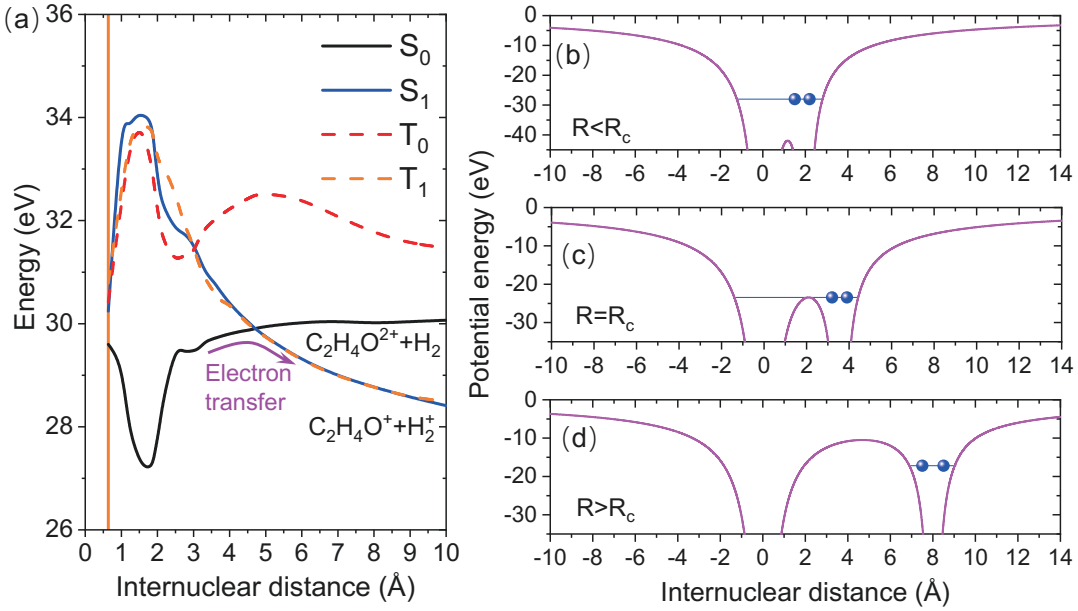


Figure 5: (a) Potential energy relative to the neutral ethanol as a function of the center-of-mass distance between $H_2$ and $C_2H_4O$ using XMS-CASPT2/(6e, 6o)/cc-pVTZ. The solid and dashed curves correspond to the singlet and triplet states, respectively. The vertical double ionization at the equilibrium geometry of ethanol (trans-conformer) is marked by the orange line. (b)-(d) Illustration of the classical over-the-barrier model for a doubly charged ion and neutral $H_2$ channel at internuclear distance smaller than the critical distance (b), equal to the critical distance (c), and larger than the critical distance (d). The bound electron ($V_{IP}$ = 15.4 eV[39]) can overcome the potential barrier at internuclear distances smaller than the critical distance ($R_C$ = 3.6 Å).

complete-active-space second-order perturbation theory (XMS-CASPT2)[40] with cc-pVTZ basis set, which is the same method as previously used by Luzon et al.[32] and Livshits et al.[18] to study charge separation in the methanol dication. The result is shown in Fig. 5 (a), where the solid and dashed curves correspond to the singlet and triplet states, and the orange vertical line indicates vertical double ionization at the equilibrium geometry. The adiabatic potential energy curves up to the fourth excited state are shown in the Supporting Information section IV. Similar to the dication of methanol, the triplet state has a very high potential barrier of about 4 eV which creates a metastable dication.[41] It is almost barrierless for the ground singlet dissociating into $H_2$ + $C_2H_4O^{2+}$ or $H_2^+$ + $C_2H_4O^+$ charge separation channel. The deep potential well on the solid black curve at about 1.7 Å corresponds to $H_2$ formation. The same electronic configuration will lead to the $H_2$ + $C_2H_4O^{2+}$ channel. At the dissociation limit, the charge separation channel has a lower total energy, therefore, the adiabatic potential energy curve results in the Coulomb explosion channel of $H_2^+$ + $C_2H_4O^+$. The charge separation COM is determined by the crossing point, which is 4.7 Å. Both the *ab initio* potential energy curve and the Coulomb explosion model give a KER of 3.1 eV for $H_2^+$ + $C_2H_4O^+$, as shown by the red line in Fig. 3 (a). The COM distance of PT (3.7 Å)[33] is shorter than that of the ET (4.7 Å), which results in a higher peak KER value for PT, as shown in Fig. 3 (a) and (b). For a reference, the potential energy of channel $C_2H_3O^+$ + $H_3^+$ as a function of the reaction coordinates is shown in Figure 4 of the publication of Wang et al.[33]

From a classical point of view, ET can be understood by the classical OTB model,[1,2] as shown in Fig. 5 (b)-(d). The solid purple curves represent the potential energy barrier as a function of internuclear distance calculated by the classical OTB model, and the blue lines indicate the ionization potential of the neutral $H_2$ in the presence of the Coulomb field of the dicationic cofragment. In the classical OTB model, the potential energy barrier is described by

$$V_e(r, R) = -\frac{p^*}{R - r} - \frac{q}{r} \tag{1}$$

where $p^*$ and $q$ are the effective charges of the electron donor and acceptor, and $r$ and $R$ are the electron and nuclear coordinates, respectively. As shown by the blue solid line in Fig. 5 (b), the electron is shared between the two moieties as long as its binding energy is higher than the maxima of the potential barrier. The ET critical distance $R_c$, shown in Fig. 5 (c), is determined by matching the binding energy in the presence of the Coulomb potential and the maxima of the potential barrier,

$$R_c = \frac{p^* + 2\sqrt{p^* q}}{|E_i|} \tag{2}$$

where $E_i = 15.4$ eV[39] is the binding energy of $H_2$. As shown in Fig. 5 (d), the electron is classically localized at $H_2$ while the internuclear distance is longer than the critical distance. Using the OTB, the critical distance is determined to be $R_C = 3.6$ Å , which is smaller than the value from the *ab initio* calculation (4.7 Å) since we assume a point charge for the dication. The KER predicted from the classical OTB model is 4.0 eV, which is within the experimental KER range, as shown by the green line in Fig. 3 (a).

It is worthwhile to note that at small internuclear distances of the classical OTB model, the electron of $H_2$ is shared by the two moieties, and we may only get the $H_2^+ + C_2H_4O^+$ channel once the $H_2$ is ejected from the parent ion. However, the *ab initio* calculations indicate that there is a gap between the potential energy curves of $H_2 + C_2H_4O^{2+}$ and $H_2^+ + C_2H_4O^+$ channels at an internuclear distance smaller than the critical distance. In this case, there is no orbital overlap between $H_2$ and $C_2H_4O^{2+}$ which prevents the ET.

In summary, we have studied the ultrafast roaming and charge separation dynamics in ethanol using a combination of XUV FEL pump-probe spectroscopy and Coulomb explosion imaging. We observed a change in the yield ratio of $H_3^+$ to $H_2^+$ as a function of time delay. Through the use of *ab initio* molecular dynamics simulations, we were able to attribute this behavior to be due to a competition of electron and proton transfer between the roaming $H_2$ and $C_2H_4O^{2+}$. A similar observation has also recently been found in the dissociative

ionization of methanol by Gope et al.[20] The present work shows the evidence in the case of larger molecule, ethanol. Furthermore, these findings might be a general phenomenon where molecular decay channels with comparable timescales could show a similar competition.

# Methods

The experiment was carried out using the Reaction Microscope (ReMi) endstation at beamline FL26 of the FLASH2 free-electron laser in Hamburg. The effective repetition frequency of the FEL pulses was 201 Hz, which corresponds to roughly 5 microseconds spacing between the pulses in a pulse train, and each pulse had a pulse length of approximately 60 fs. The details of the experimental setup shown in Fig. 1 (b) have been described elsewhere[42] and only a brief summary is given here. The ethanol jet was generated by a supersonic gas expansion of ethanol vapor at room temperature. The gas expanded into the vacuum chamber through a 30 $\mu$m diameter nozzle and was collimated by two skimmers with 180 and 400 $\mu$m diameter, respectively. A split mirror split the incoming FEL beam into two identical pulses with an average pulse energy of about 6 $\mu$J. The time delay between the pulses was controlled by moving one of the halves of the split mirror. Subsequently, the two beams were focused by the ellipsoidal mirror into the supersonic gas jet. The ions created by the interaction with the FEL pulses were projected to the temporal- and position-sensitive delay-line detector by a homogeneous electric field of 40 $\mathrm{Vcm}^{-1}$. The three-dimensional momentum vectors of all detected charged fragments were reconstructed by their detected time-of-flight and positions.

The molecular dynamical simulations were performed as follows: (i) in the first step, the initial geometries and velocities of every atom of neutral ethanol were sampled by the quasi-classical fixed normal-mode sampling method.[43] (ii) In the second step, we assume a vertical double ionization from the neutral to the dicationic state and the molecular dynamics simulation of the dication was performed using the atom-centered density matrix propagation

(ADMP) method[44–46] using the density-functional theory method at B3LYP/cc-pVDZ level. Since the experiment was performed with a supersonic gas jet where the target temperature is lower than room temperature, the temperature for which we did the sampling in step (i) was estimated to be 100 K. The fictitious electronic mass was 0.1 amu, and the simulation time step was 0.5 fs. Both of the two conformers of ethanol (trans- and gauche-conformer) were included in the sampling process, and 1000 trajectories were simulated for every conformer. At the end of the simulation, the Mulliken charges of every atom were calculated. Only those $H_2$ with a charge less than 0.5 $e^-$ are regarded as a neutral state and their trajectories are analyzed.

# Acknowledgement

We gratefully acknowledge the scientific and technical team at FLASH for their hospitality and support during the beamtime and for the excellent operation of the FEL. This work was funded by the Chemical Sciences, Geosciences and Biosciences Division, Office of Basic Energy Sciences, Office of Science, US Department of Energy, grant nos. DE-SC0012376 (N.G.K., A.C.L,, R.O. and N.B.), DE-FG02-86ER13491 (E.W., S.P., A.R., D.R.), and DE-SC0020276 (S.B.). S.P. was also partially supported by the National Science Foundation (NSF) Grant No. PHYS-1753324 to D.R. E.W. was partially supported by the Strategic Priority Research Program of Chinese Academy of Sciences (Grant No. XDB34020000), the CAS Pioneer Hundred Talents Program, and the USTC Research Funds of the Double First-Class Initiative. S.D-T and F.M's contribution is based upon work from COST actions CA18212 - Molecular Dynamics in the GAS phase (MD-GAS), and CA18222 - Attosecond Chemistry (AttoChem), supported by COST (European Cooperation in Science and Technology). Their work was also partially supported by MICINN (Spanish Ministry of Science and Innovation) projects PID2019-105458RB-I00 and PID2019-110091GB-I00, funded by MCIN/AEI/10.13039/501100011033, the 'Severo Ochoa' Programme for Centres of Ex-

cellence in R & D (CEX2020-001039-S) and the 'María de Maeztu' Programme for Units of Excellence in R & D (CEX2018-000805-M). We acknowledge the generous allocation of computer time at the Centro de Computación Científica at the Universidad Autónoma de Madrid (CCC-UAM).

# Supporting Information

**Supporting Information Available:** Kinetic energy vs. delay spectrum; Kinetic energy release of $H_2 + C_2H_4O^{2+}$ and $H_2^+ + C_2H_4O^+$ channels at FEL energies of 28 eV, 32 eV and 70 eV; PIPICO spectrum; Adiabatic potential energy curve.

# References

(1) Schnorr, K.; Senftleben, A.; Kurka, M.; Rudenko, A.; Schmid, G.; Pfeifer, T.; Meyer, K.; Kübel, M.; Kling, M. F.; Jiang, Y. H. et al. Electron Rearrangement Dynamics in Dissociating $I_2^{n+}$ Molecules Accessed by Extreme Ultraviolet Pump-Probe Experiments. *Phys. Rev. Lett.* **2014**, *113*, 073001.

(2) Erk, B.; Boll, R.; Trippel, S.; Anielski, D.; Foucar, L.; Rudek, B.; Epp, S. W.; Coffee, R.; Carron, S.; Schorb, S. et al. Imaging Charge Transfer in Iodomethane upon X-ray Photoabsorption. *Science* **2014**, *345*, 288–291.

(3) Motomura, K.; Kukk, E.; Fukuzawa, H.; Wada, S.-i.; Nagaya, K.; Ohmura, S.; Mondal, S.; Tachibana, T.; Ito, Y.; Koga, R. et al. Charge and Nuclear Dynamics Induced by Deep Inner-Shell Multiphoton Ionization of $CH_3I$ Molecules by Intense X-ray Free-Electron Laser Pulses. *J. Phys. Chem. Lett.* **2015**, *6*, 2944–2949.

(4) Boll, R.; Erk, B.; Coffee, R.; Trippel, S.; Kierspel, T.; Bomme, C.; Bozek, J. D.; Burkett, M.; Carron, S.; Ferguson, K. R. et al. Charge Transfer in Dissociating Iodomethane

and Fluoromethane Molecules Ionized by Intense Femtosecond X-ray Pulses. *Struct. Dyn.* **2016**, *3*, 043207.

(5) Rudenko, A.; Inhester, L.; Hanasaki, K.; Li, X.; Robatjazi, S. J.; Erk, B.; Boll, R.; Toyota, K.; Hao, Y.; Vendrell, O. et al. Femtosecond Response of Polyatomic Molecules to Ultra-intense Hard X-rays. *Nature* **2017**, *546*, 129–132.

(6) Hollstein, M.; Mertens, K.; Klumpp, S.; Gerken, N.; Palutke, S.; Baev, I.; Brenner, G.; Dziarzhytski, S.; Meyer, M.; Wurth, W. et al. Ultrafast Charge Redistribution in Small Iodine Containing Molecules. *New J. Phys.* **2019**, *21*, 033017.

(7) Rousseau, P.; González-Vázquez, J.; Piekarski, D. G.; Kopyra, J.; Domaracka, A.; Alcamí, M.; Adoui, L.; Huber, B. A.; Díaz-Tendero, S.; Martín, F. Timing of Charge Migration in Betaine by Impact of Fast Atomic Ions. *Sci. Adv.* **2021**, *7*, eabg9080.

(8) Attar, A. R.; Bhattacherjee, A.; Pemmaraju, C. D.; Schnorr, K.; Closser, K. D.; Prendergast, D.; Leone, S. R. Femtosecond X-ray Spectroscopy of an Electrocyclic Ring-opening Reaction. *Science* **2017**, *356*, 54–59.

(9) Rudakov, F.; Weber, P. M. Ultrafast Structural and Isomerization Dynamics in the Rydberg-exited Quadricyclane: Norbornadiene System. *J. Chem. Phys.* **2012**, *136*, 134303.

(10) Maclot, S.; Piekarski, D. G.; Domaracka, A.; Méry, A.; Vizcaino, V.; Adoui, L.; Martín, F.; Alcamí, M.; Huber, B. A.; Rousseau, P. et al. Dynamics of Glycine Dications in the Gas Phase: Ultrafast Intramolecular Hydrogen Migration versus Coulomb Repulsion. *J. Phys. Chem. Lett.* **2013**, *4*, 3903–3909.

(11) Kling, N. G.; Díaz-Tendero, S.; Obaid, R.; Disla, M. R.; Xiong, H.; Sundberg, M.; Khosravi, S. D.; Davino, M.; Drach, P.; Carroll, A. M. et al. Time-resolved Molecular Dynamics of Single and Double Hydrogen Migration in Ethanol. *Nat. Commun. 10*, 2813.

(12) McDonnell, M.; LaForge, A. C.; Reino-González, J.; Disla, M.; Kling, N. G.; Mishra, D.; Obaid, R.; Sundberg, M.; Svoboda, V.; Díaz-Tendero, S. et al. Ultrafast Laser-Induced Isomerization Dynamics in Acetonitrile. *J. Phys. Chem. Lett.* **2020**, *11*, 6724–6729.

(13) Mishra, D.; Reino-González, J.; Obaid, R.; LaForge, A. C.; Díaz-Tendero, S.; Martín, F.; Berrah, N. Ultrafast Molecular Dynamics in Ionized 1- and 2-propanol: from Simple Fragmentation to Complex Isomerization and Roaming Mechanisms. *Phys. Chem. Chem. Phys.* **2022**, *24*, 433–443.

(14) Calegari, F.; Ayuso, D.; Trabattoni, A.; Belshaw, L.; Camillis, S. D.; Anumula, S.; Frassetto, F.; Poletto, L.; Palacios, A.; Decleva, P. et al. Ultrafast Electron Dynamics in Phenylalanine Initiated by Attosecond Pulses. *Science* **2014**, *346*, 336–339.

(15) Florián, J.; Leszczyński, J. Spontaneous DNA Mutations Induced by Proton Transfer in the Guanine Cytosine Base Pairs: An Energetic Perspective. *J. Am. Chem. Soc. 118*, 3010–3017.

(16) Ekanayake, N.; Severt, T.; Nairat, M.; Weingartz, N. P.; Farris, B. M.; Kaderiya, B.; Feizollah, P.; Jochim, B.; Ziaee, F.; Borne, K. et al. $H_2$ Roaming Chemistry and the Formation of $H_3^+$ from Organic Molecules in Strong Laser Fields. *Nat. Commun.* **2018**, *9*, 5186.

(17) Ekanayake, N.; Nairat, M.; Weingartz, N. P.; Michie, M. J.; Levine, B. G.; Dantus, M. Substituent Effects on $H_3^+$ Formation via $H_2$ Roaming Mechanisms from Organic Molecules under Strong-field Photodissociation. *J. Chem. Phys.* **2018**, *149*, 244310.

(18) Livshits, E.; Luzon, I.; Gope, K.; Baer, R.; Strasser, D. Time-resolving the Ultrafast $H_2$ Roaming Chemistry and $H_3^+$ Formation Using Extreme-ultraviolet Pulses. *Commun. Chem.* **2020**, *3*, 1–6.

(19) Townsend, T.; Schwartz, C. J.; Jochim, B.; P., K. R.; Severt, T.; Iwamoto, N.; Napier-

ala, J. L.; Feizollah, P.; Tegegn, S. N.; Solomon, A. et al. Controlling $H_3^+$ Formation From Ethane Using Shaped Ultrafast Laser Pulses. *Front. Phys.* **2021**, *9*.

(20) Gope, K.; Livshits, E.; Bittner, D. M.; Baer, R.; Strasser, D. An "inverse" Harpoon Mechanism. *Sci. Adv.* **2022**, *8*, eabq8084.

(21) Townsend, D.; Lahankar, S. A.; Lee, S. K.; Chambreau, S. D.; Suits, A. G.; Zhang, X.; Rheinecker, J.; Harding, L. B.; Bowman, J. M. The Roaming Atom: Straying from the Reaction Path in Formaldehyde Decomposition. *Science* **2004**, *306*, 1158–1161.

(22) Endo, T.; Neville, S. P.; Wanie, V.; Beaulieu, S.; Qu, C.; Deschamps, J.; Lassonde, P.; Schmidt, B. E.; Fujise, H.; Fushitani, M. et al. Capturing Roaming Molecular Fragments in Real Time. *Science* **2020**, *370*, 1072–1077.

(23) Thürmer, S.; Ončák, M.; Ottosson, N.; Seidel, R.; Hergenhahn, U.; Bradforth, S. E.; Slavíček, P.; Winter, B. On the Nature and Origin of Dicationic, Charge-separated Species Formed in Liquid Water on X-ray Irradiation. *Nat. Chem.* **2013**, *5*, 590–596.

(24) Schwaab, G.; Pérez de Tudela, R.; Mani, D.; Pal, N.; Roy, T. K.; Gabas, F.; Conte, R.; Durán Caballero, L.; Ceotto, M.; Marx, D. et al. Zwitter Ionization of Glycine at Outer Space Conditions due to Microhydration by Six Water Molecules. *Phys. Rev. Lett.* **2022**, *128*, 033001.

(25) Oka, T. Interstellar $H_3^+$. *P. Natl. Acad. Sci. USA* **2006**, *103*, 12235–12242.

(26) Wang, E.; Ren, X.; Dorn, A. Role of the Environment in Quenching the Production of $H_3^+$ from Dicationic Clusters of Methanol. *Phys. Rev. Lett.* **2021**, *126*, 103402.

(27) Mi, Y.; Wang, E.; Dube, Z.; Wang, T.; Naumov, A. Y.; Villeneuve, D.; Corkum, P.; Staudte, A. Observation and Dynamic Control of a New Pathway of $H_3^+$ Formation. *arXiv preprint arXiv:2209.00203* **2022**,

(28) Marsalek, O.; Elles, C. G.; Pieniazek, P. A.; Pluhařová, E.; VandeVondele, J.; Bradforth, S. E.; Jungwirth, P. Chasing Charge Localization and Chemical Reactivity Following Photoionization in Liquid Water. *J. Chem. Phys.* **2011**, *135*, 224510.

(29) Piekarski, D. G.; Delaunay, R.; Maclot, S.; Adoui, L.; Martín, F.; Alcamí, M.; Huber, B. A.; Rousseau, P.; Domaracka, A.; Díaz-Tendero, S. Unusual Hydroxyl Migration in the Fragmentation of $\beta$-alanine Dication in the Gas Phase. *Phys. Chem. Chem. Phys.* **2015**, *17*, 16767–16778.

(30) Richter, C.; Hollas, D.; Saak, C.-M.; Förstel, M.; Miteva, T.; Mucke, M.; Björneholm, O.; Sisourat, N.; Slavíček, P.; Hergenhahn, U. Competition between Proton Transfer and Intermolecular Coulombic Decay in Water. *Nat. Commun.* **2018**, *9*, 4988.

(31) Cederbaum, L. S.; Zobeley, J.; Tarantelli, F. Giant Intermolecular Decay and Fragmentation of Clusters. *Phys. Rev. Lett.* **1997**, *79*, 4778–4781.

(32) Luzon, I.; Livshits, E.; Gope, K.; Baer, R.; Strasser, D. Making Sense of Coulomb Explosion Imaging. *J. Phys. Chem. Lett.* **2019**, *10*, 1361–1367.

(33) Wang, E.; Shan, X.; Chen, L.; Pfeifer, T.; Chen, X.; Ren, X.; Dorn, A. Ultrafast Proton Transfer Dynamics on the Repulsive Potential of the Ethanol Dication: Roaming-Mediated Isomerization versus Coulomb Explosion. *J. Phys. Chem. A* **2020**, *124*, 2785–2791.

(34) Linusson, P.; Stenrup, M.; Larson, A.; Andersson, E.; Heijkenskjöld, F.; Andersson, P.; Eland, J. H. D.; Karlsson, L.; Rubensson, J.-E.; Feifel, R. Double Photoionization of Alcohol Molecules. *Phys. Rev. A* **2009**, *80*, 032516.

(35) Ning, C. G.; Luo, Z. H.; Huang, Y. R.; Hajgató, B.; Morini, F.; Liu, K.; Zhang, S. F.; Deng, J. K.; Deleuze, M. S. Investigation of the Molecular Conformations of Ethanol Using Electron Momentum Spectroscopy. *J. Phys. B* **2008**, *41*, 175103.

(36) Barillot, T.; Alexander, O.; Cooper, B.; Driver, T.; Garratt, D.; Li, S.; Al Haddad, A.; Sanchez-Gonzalez, A.; Agåker, M.; Arrell, C. et al. Correlation-Driven Transient Hole Dynamics Resolved in Space and Time in the Isopropanol Molecule. *Phys. Rev. X* **2021**, *11*, 031048.

(37) Lavín, C.; Vega, M. V.; Velasco, A. M. Photoionization Cross Sections and Asymmetry Parameters for the Valence Shell of Methanol. *J. Phys. Chem. A* **2012**, *116*, 11913–11919.

(38) Gope, K.; Bittner, D. M.; Strasser, D. Sequential Mechanism in $H_3^+$ Formation Dynamics on the Ethanol Dication. *Phys. Chem. Chem. Phys.* **2023**, *25*, 6979–6986.

(39) NIST Chemistry WebBook, SRD 69. https://webbook.nist.gov/cgi/cbook.cgi?ID=C1333740&Mask=20.

(40) Shiozaki, T. BAGEL: Brilliantly Advanced General Electronic-structure Library. *WIREs Computational Molecular Science* **2018**, *8*, e1331.

(41) Gope, K.; Livshits, E.; Bittner, D. M.; Baer, R.; Strasser, D. Absence of Triplets in Single-Photon Double Ionization of Methanol. *J. Phys. Chem. Lett.* **2020**, *11*, 8108–8113.

(42) Schmid, G.; Schnorr, K.; Augustin, S.; Meister, S.; Lindenblatt, H.; Trost, F.; Liu, Y.; Braune, M.; Treusch, R.; Schröter, C. D. et al. Reaction Microscope Endstation at FLASH2. *J. Synchrotron Radiat.* **2019**, *26*, 854–867.

(43) M. J. Frisch, *et al.* , Gaussian 16 Revision A.03. 2016; Gaussian Inc. Wallingford CT.

(44) Schlegel, H. B.; Millam, J. M.; Iyengar, S. S.; Voth, G. A.; Daniels, A. D.; Scuseria, G. E.; Frisch, M. J. Ab Initio Molecular Dynamics: Propagating the Density Matrix with Gaussian Orbitals. *J. Chem. Phys.* **2001**, *114*, 9758–9763.

(45) Iyengar, S. S.; Schlegel, H. B.; Millam, J. M.; Voth, G. A.; Scuseria, G. E.; Frisch, M. J. Ab Initio Molecular Dynamics: Propagating the Density Matrix with Gaussian Orbitals. II. Generalizations Based on Mass-weighting, Idempotency, Energy conservation and Choice of Initial Conditions. *J. Chem. Phys.* **2001**, *115*, 10291–10302.

(46) Schlegel, H. B.; Iyengar, S. S.; Li, X.; Millam, J. M.; Voth, G. A.; Scuseria, G. E.; Frisch, M. J. Ab Initio Molecular Dynamics: Propagating the Density Matrix with Gaussian Orbitals. III. Comparison with Born-Oppenheimer Dynamics. *J. Chem. Phys.* **2002**, *117*, 8694–8704.